Flexible Multi-wideband Wearable Antenna for Preliminary Evaluation of Tumour Detection in Breast Phantom Model

Sheng Chong Chua[1], Raimi Dewan[1,2,3], Faishal Adilah Suryanata[2],Man Seng Sim[4], Maria Alessandra Sabiniano Florida[1],Kok Yeow You[4] and Mohamad Kamal A Rahim[2,4]

[1]Department of Biomedical Engineering and Health Sciences Faculty of Electrical Engineering, Universiti Teknologi Malaysia, 81310 UTM Johor Bahru, Johor, Malaysia
[2]Advanced Radio Frequency & Microwave Research Group, Faculty of Electrical Engineering, Universiti Teknologi Malaysia, 81310 UTM Johor Bahru, Johor, Malaysia
[3]IJN-UTM Cardiovascular Engineering Centre, Institute of Human Centered Engineering, Universiti Teknologi Malaysia, 81310 UTM Johor Bahru, Johor, Malaysia
[4] Department of Communication Engineering, Faculty of Electrical Engineering, Universiti Teknologi Malaysia, 81310 Johor Bahru, Johor, Malaysia

Corresponding author: Raimi Dewan (email: raimi.dar@utm.my)

ABSTRACT The growing demand for non-invasive and wearable breast cancer diagnostic tools has driven the development of flexible and wearable antennas for microwave imaging. This study presents a flexible multi-wideband wearable antenna designed for breast tumour detection, with targeted operation at the 2.4 GHz Industrial, Scientific, and Medical (ISM) band for deep tissue penetration and a wideband response above 5.04 GHz for high-resolution sensing which fabricated on a breathable cotton substrate with a 0.035 mm copper layer, the antenna measures 83 × 60 × 1.52 mm³ and is backed by a 2×3 Artificial Magnetic Conductor (AMC) array to enhance the gain whilst suppressing back radiation. Simulations and measurements are conducted in free space and on a realistic three-layer breast phantom consisting of skin, fat and glandular which is properly characterise in terms of electrical parameter has successfully, demonstrate a directional radiation, strong resonance at 2.4 GHz and wideband performance above 5.04 GHz. The antenna exhibits insensitivity to bending angle up to 60° and exhibits a low Specific Absorption Rate (SAR) value of 0.23 W/kg (10 g), ensuring safety compliance for wearable use to human skin proximity. While the current design supports tumour detection with varying sizes between 2–10 mm, future work will focus on extending the bandwidth below 5 GHz and miniaturizing the structure for enhanced early-stage diagnosis.

INDEX TERMS Artificial Magnetic Conductor (AMC), Breast tumour detection, Directional radiation, Specific Absorption Rate (SAR), Wearable antenna

I. INTRODUCTION

Breast cancer occurs when cells in the breast grow uncontrollably and can spread to other parts of the body. In 2020, breast cancer accounted for approximately 685,000 deaths globally, making it the second leading cause of mortality among women [1]. However, early detection can increase survival rates by up to 97%, highlighting the need for improved screening methods.

Existing breast imaging techniques such as mammography, ultrasound, Positron Emission Tomography (PET) and Magnetic Resonance Imaging (MRI) have limitations. Mammography can lead to unnecessary treatments, ultrasound has low spatial resolution, and MRI is expensive and may produce false negatives [2]. These drawbacks have driven interest in non-ionizing, low-cost, and non-invasive alternatives such as microwave imaging.

Microwave imaging detects tumours by exploiting dielectric property differences between normal and cancerous tissues [4]. Cancerous tissues have higher relative permittivity and conductivity compared to healthy tissues due to increased water content [5], which enables detection using reflected microwave signals. Among various techniques, UWB radar imaging has emerged as a promising approach [3].

Antennas play a crucial role in microwave imaging systems. Wearable UWB antennas require a practical compromise between delivering high electromagnetic performance and remaining flexible, comfortable and safe for continuous use on the human body even under movement situation. [1,2]. Additionally, designs should conform to breast contours, minimize signal distortion and support wide bandwidth [6]. However, many existing wideband antennas—such as circular, Vivaldi, and Bowtie types exhibit omnidirectional radiation and low gain, limiting their

effectiveness in terms of directivity, imaging resolution, and energy focusing [7]. While antenna arrays offer better detection due to their sequential detection and localization approach [9], such design often suffer from bulkiness, complex feeding networks that may incurred additional losses contributed by feeding lines and impedance matching and fabrication challenges associated by having multiple elements, feeding networks and especially in a structure consisting of multiple substrate application [9].

Several recent UWB wearable antenna designs from previous studies, exhibit common limitations such as large physical dimensions [9], complex structures and poor mechanical strength. Furthermore, many of these antennas exhibit energy omnidirectionally [7], reducing focus on the tumour region and reducing detection performance. In an omnidirectional design, the radiated energy is dispersed equally in all directions, causing only a limited portion of the field to penetrate the breast tissue where the tumour may be located. This results in weaker interaction with the target region, lower signal-to-noise ratio, and less pronounced transmission or reflection changes, making it more difficult to accurately detect or localize tumours.

This study designs propose a flexible multi-wideband wearable antenna that operates on a breast phantom model to detect breast tumours using S-parameters measurements at 2.4 GHz. The antenna is optimized for an improved return loss, minimizing the effects of bending and structural deformations. Additionally, the antenna is fabricated and tested to evaluate its performance in terms of radiation pattern and Specific Absorption Rate (SAR), to ensure safety for microwave imaging applications.

This article is divided into sections: Design and analysis of flexible multi-wideband antenna are discussed in section II. Simulated and measured results of flexible multi-wideband antenna, in terms of *S*-parameters and radiation pattern in section III, comparison of the proposed multi-wideband antenna with existing antennas are discussed in section IV. And the conclusion is stated in section V.

II. MULTI-WIDEBAND ANTENNA DESIGN METHODOLOGY

A. ANTENNA DESIGN COMPONENTS

The wearable antenna design prioritized user comfort, given its intended direct placement on the human breast. Therefore, materials were selected for their flexibility, electrical performance. This section details the conductive and substrate materials used, along with the microstrip feeding technique and SubMiniature version A (SMA) connector integration.

Copper was selected as the conductive material for both the radiating patch and ground plane of the antenna due to its high electrical conductivity (5.8×10^7 S/m) and mechanical flexibility, which enables the antenna to withstand deformation without compromising performance when worn on the human body [10], [11]. A copper sheet with a thickness of 0.035 mm was used in the fabrication, consistent with the material properties available in the CST simulation library.

Cotton was chosen as the dielectric substrate due to its flexibility and comfort for direct skin contact [12]. This material selection is supported by recent advancements in flexible antenna technology. Previous studies have demonstrated that textile materials, such as fleece used in flexible UWB antennas for RFID, are highly effective for body-centric communications due to the ergonomic nature and conform to non-planar surfaces. The flexibility may ensure the antenna will maintain the performance even when bent or wrapped around the breast model [22]. To accurately model the dielectric properties of the material, the relative permittivity and loss tangent from 1 GHz to 9 GHz were measured using a Keysight FieldFox Microwave Vector Network Analyzer (N9925A) equipped with a dielectric probe kit. Prior to measurement, standard calibration using open, short, and load standards was performed for the coaxial cables, followed by calibration using air, Teflon, and water for the dielectric probe to ensure measurement accuracy.

Layers of cotton were compressed to form a 3 mm-thick cotton stack, minimizing the presence of air gaps and ensuring conformity with equipment specifications and measurement tolerances. This thickness was selected to provide reliable and repeatable results during testing. The dielectric measurement was repeated 10 times on different points of the cotton stack. The measured permittivity ranged from approximately 2.2–2.4 (1–4 GHz) and 2.0–2.2 (4–9 GHz). Besides, recalibration was conducted when changing frequency ranges to maintain consistency. At 2.4 GHz, the measured relative permittivity and loss tangent were 2.4608 and 0.1404 respectively. These values were input as the material electrical parameters for the cotton substrate in the simulation model.

The antenna structure was developed using high-conductivity copper for both the outer and inner conductors, with a conductivity of 5.8×10^7 S/m. The dielectric material selected for the substrate was polytetrafluoroethylene (PTFE), which offers a low relative permittivity of 2.1, contributing to stable and efficient signal performance. To ensure proper signal excitation and impedance matching, the antenna was fed using a 50-ohm microstrip line with a 2 mm width. A SMA connector was employed to connect the microstrip feed with external Radio Frequency (RF) systems, enabling reliable transmission and measurement of RF signals [13].

B. EVOLUTION OF MULTI-WIDEBAND ANTENNA

The evolution of the multi-wideband antenna is illustrated in Figure 1. The designed antenna consists of radiation patch printed on the flexible substrate, cotton with thickness of t = 0.08 mm. The dimension of the substrate is 83 mm × 60 mm × 1.52 mm (the cotton is combined up to 10 layers and included with air gaps, which same thickness t with the substrate). Polyester copper tape with 0.035 mm thickness was used as the conductive material.

As shown in Figure 1(a), the initial antenna was adapted from previously published designs [7] and design modification and optimisation is done by introducing a staircase-shaped radiation patch intended at achieving ultra-wideband (UWB) performance. The preliminary model which simulated in free space, demonstrated a poor impedance bandwidth ranging from 1–12 GHz due to the single layer cotton substrate as the bandwidth would be affected by the substrate thickness. According to the bandwidth equation shown in equation (1) for microstrip antennas [14], the substrate thickness h is directly proportional to the operating bandwidth (BW). This indicates that increasing the substrate thickness contributes to a wider bandwidth [14]. A parametric sweep was carried out, varying the number of cotton layers from 5 to 10. As depicted in Figure 2, the configuration with 10 layers exhibited the most optimal S_{11} response with significant improvement in impedance bandwidth, proof that thicker substrate could enhance the bandwidth.

$$\mathrm{BW} = \frac{16}{3\sqrt{2}} \cdot \frac{p}{\varepsilon_r \cdot \varepsilon_r} \cdot \frac{h}{\lambda_0} \cdot \frac{W}{L} \cdot \frac{1}{q} \tag{1}$$

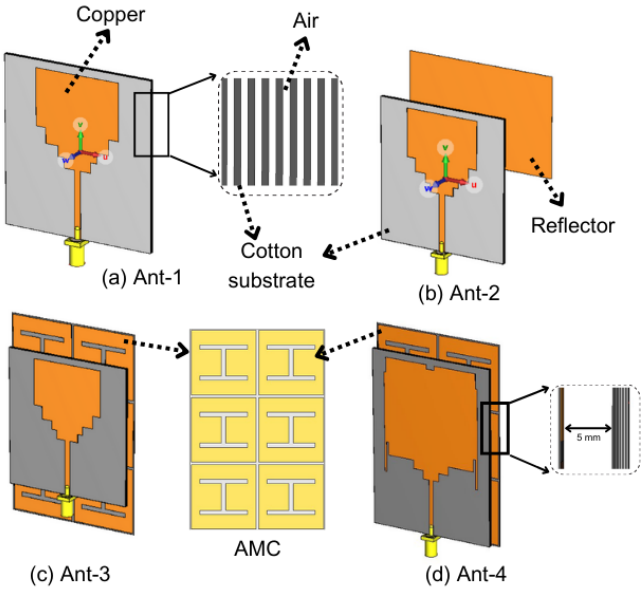

FIGURE 1. Design progression of multi-wideband antenna (a) Ant-1, (b) Ant-2, (c) Ant-3, (d) Ant-4

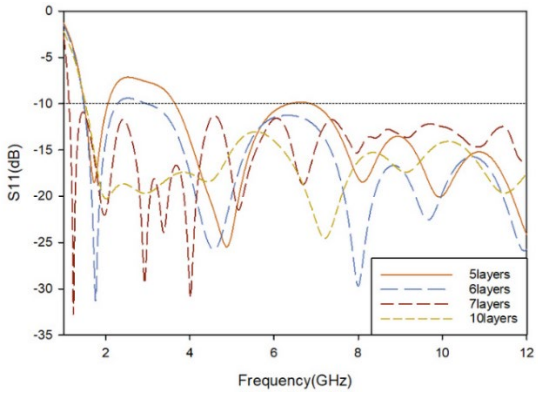

FIGURE 2. Parametric sweep of multi-layered of cotton layers

Despite the improved reflection coefficient, S_{11}, the radiation pattern remained omnidirectional. To introduce directionality, a planar copper reflector (70 mm × 46 mm × 0.035 mm) was placed 31.25 mm below the antenna, as illustrated in Figure 1(b). This corresponds to a quarter-wavelength (λ/4) spacing at 2.4 GHz, producing constructive interference from the reflected wave to shape the beam into a bidirectional pattern. The reflector significantly enhanced the forward gain to 4.58 dBi. However, the bulky air gap causes the design impractical for wearable applications, especially placed on human breast.

To address this limitation, an Artificial Magnetic Conductor (AMC) was introduced below the antenna as depicted in Figure 1(c). The AMC is a metamaterial structure engineered to mimic a Perfect Magnetic Conductor (PMC), which does not exist in nature. Unlike standard Perfect Electric Conductor (PEC) ground planes that reflect waves with a 180° phase shift (causing destructive interference when placed close to the antenna), an AMC provides a zero-degree reflection phase at its resonant frequency [21]. Although in theory, the antenna can be placed directly on the AMC surface to achieve in-phase reflection at resonance, this approach is impractical due to near-field coupling and impedance mismatch [15]. Therefore, minimal separation must be maintained between the antenna and the AMC to ensure optimal performance. In this work, a very thick foam layer is inserted to create the necessary air gap.

A compact I-slot AMC unit cell with dimensions of 31.5 mm × 31.5 mm × 0.08 mm was designed by modifying a conventional rectangular patch as shown in Figure 3 and its reflection phase shown in Figure 4 while the exact dimensions are listed in Table I. A 2×3 AMC array was found optimal after various configurations of AMC arrays (2×3, 3×3, 4×4) and air gaps (2–5 mm). The AMC with a 5 mm air gap equivalent to 0.04λ, offered the best trade-off, producing a directional radiation pattern with positive gain and reduced backward radiation.

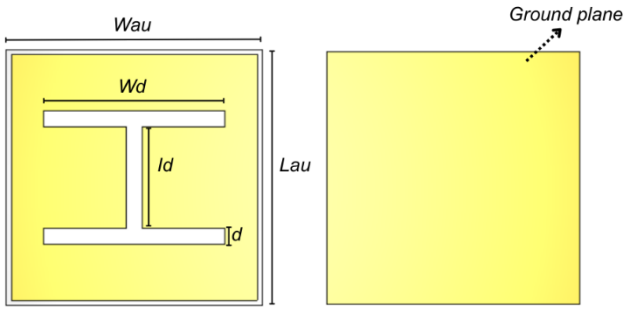

FIGURE 3. (a) The front and (b) back view of the final AMC unit cell design

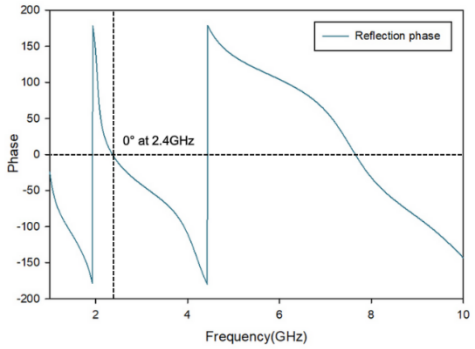

FIGURE 4. Reflection phase of AMC design

TABLE I. Dimensions of proposed AMC design

Parameter	Size (mm)
Wau, Lau	31.50
h	0.08
Gh, Ph	0.035
D	2.00
Ld	12.50
Wd	22.30

Subsequent optimization focused on the antenna performance specifically for 2.4 GHz operation. Parametric tuning was conducted on key dimensions including substrate length, patch width and slot placements. The increasement of the substrate length could shifted the resonance frequency to 2.4 GHz, while introducing slots at the edges of the radiation patch effectively minimizes the S_{11} value thereby enhancing impedance matching at the resonance frequencies of 2.4 GHz and 5.71 GHz.

The final antenna design, referred to as Ant-4 and illustrated in Figure 1(d), integrates all proposed structural optimizations to enhance both impedance and radiation performance. The precise physical dimensions of the design are provided in Figure 2 and Table II.

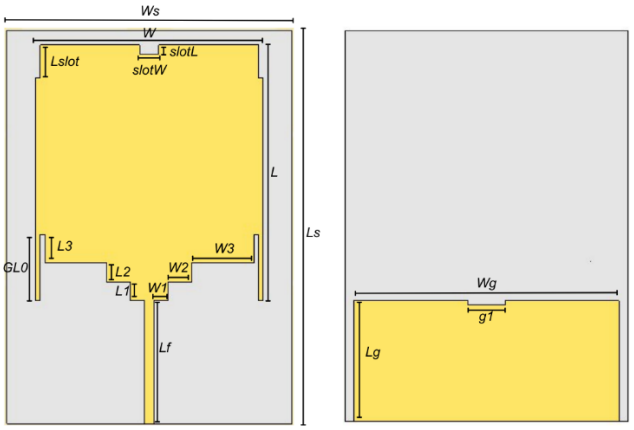

FIGURE 5. (a) The front and (b) back view of the final antenna design (Ant-4)

TABLE II. Dimensions of proposed multi-wideband antenna

Parameter	Size (mm)	Parameter	Size(mm)
Ws	60	*W*	48.0
Ls	83	*L1*	4.0
W1	3	*L2*	4.0
W2	5	*L3*	6.0
W3	12	*GL0*	14.0
W4	1	*L*	54.0
slotL	2	*Lg*	25.7
slotW	4	*Wg*	56.5
Lslot	7	*g1*	8.0

C. ANTENNA FABRICATION

The optimised and finalised design of antenna was fabricated; the substrate was formed by sewing 10 layers of cotton fabric of dimension 60 mm × 83 mm. The final thickness, including air gaps, was measured to be approximately 1.52 mm using a digital calliper.

Conductive elements for the radiating patch and ground plane were fabricated from copper sheets. The antenna layout was exported as a DXF file and printed at 1:1 exact scale. This template was taped onto the copper sheet and the pattern was cut using scissors and a precision knife. The completed elements were then attached to the substrate. Following this, the AMC structure was fabricated using a single cotton layer as the substrate. The copper patterns were pre-cut based on the DXF layout, were aligned and affixed onto the cotton surface as illustrated in Figure 6. The dimensions and structural parameters of the fabricated design are consistent with the specifications provided in Table I.

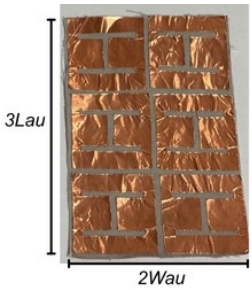

FIGURE 6. Front view of AMC

An SMA connector was mounted at the feed point to interface with the RF system. To avoid damaging the textile substrate, conductive glue was used instead of soldering. The completed antenna with SMA connector is shown in Figure 7.

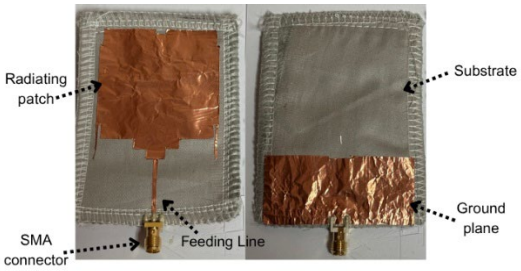

FIGURE 7. Front view and back view of fabricated antenna with SMA connector

To improve measurement stability, especially for transmission parameter denoted by S_{21} and radiation pattern analysis, a custom support holder was designed in SolidWorks and 3D-printed using a 3D printer with model Creality Ender V3 SE using PLA material as a filament. The holder illustrated in Figure 8 was fixed to the antenna dimensions and included a hole for SMA routing. This setup ensured stable placement on the breast phantom and improved measurement repeatability and stability.

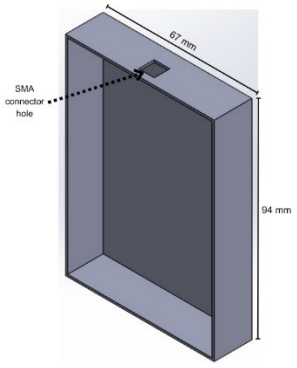

FIGURE 8. 3D design of support holder

D. BREAST AND TUMOUR PHANTOM PREPARATION

To evaluate the performance of antenna in human tissue, a multi-layered breast phantom which mimics the electrical characteristics of human breast tissue was fabricated based on the permittivity and loss tangent data extracted from prior studies primarily from reputable journals [18]. The phantom comprises of the skin, fat, and glandular tissue layers, each designed to emulate the electric properties of real breast tissues.

Three-dimensional moulds for the multilayer breast phantom were designed using SolidWorks and fabricated with a Creality Ender-3 V3 SE printer. To ensure accurate anatomical layering and prevent material leakage, separate moulds were created for each tissue layer, skin, fat and glandular. The outer skin mould was constructed with a 1.0 mm wall thickness and featured an integrated locking mechanism to provide sufficient mechanical strength and prevent leakage of phantom materials. For the fat and glandular layers, inner moulds were designed with a 0.75 mm wall thickness, which represents the minimum printable thickness that ensures watertight sealing. This precaution was critical to prevent mixing between adjacent layers, which could compromise the unique dielectric properties of each tissue type and affect key measurement parameters such as S_{21}. The inner moulds also included arm supports and alignment features to maintain structural integrity and precise positioning during assembly. Additionally, a supportive holder with anti-slip tape was employed to secure the entire mould assembly during testing.

Mixtures for each tissue layer were prepared mainly using wheat flour, distilled water and other materials, with ratios adjusted to achieve desired dielectric properties. Dyes were added to differentiate the layers visually, cream colour for skin and dark pink colour for glandular tissue, requiring further tuning of the compositions to maintain electrical consistency. Table III summarizes the final material ratios.

TABLE III. Material composition of breast phantom and tumour phantom

Material	Skin	Fat	Glandular Tissue	Tumour
NaCl	10.3 g	7.9 g	7 g	-
PPJ	-	48.00 g	-	-
Olive Oil	-	60.00 ml	-	-
Distilled water	90 ml	36 ml	41 ml	6.5 ml
Wheat Flour	108.9 g	143.2 g	123.0 g	4.3 g

Besides, to simulate a tumour, a semi-liquid phantom was prepared using 6.5 g of flour and 4.25 ml of water, mixed thoroughly and dyed orange for visibility. This mixture was sealed inside a very thin plastic glove segment using a mini heat sealer to avoid contamination of surrounding tissue layers. The sealed tumour phantom was inserted into the glandular region of the breast model to assess antenna performance in both tumour-present and tumour-absent conditions.

Once the mixtures were confirmed to meet the target permittivity, each mixture was poured into their respective moulds. The glandular mixture was blended to ensure a smooth texture. Figure 9 shows the fully assembled breast phantom with tumour phantom.

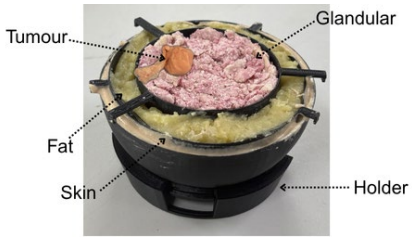

FIGURE 9. Fully assembled breast phantom with tumour

E. PERFORMANCE MEASUREMENT

To validate the performance of the fabricated antennas for breast tumour detection, both free-space and phantom-based measurements were conducted using a Vector Network Analyzer (VNA). Initially, the reflection coefficient (S_{11}) of a single antenna was measured in free space. Prior to measurement, a standard 1-port calibration was performed using open, short and load standards from a calibration kit to ensure measurement is reliable prior to performing. Successful calibration was confirmed when the VNA displayed a flat trace at the reference level. The antenna was connected to the VNA via an SMA connector and coaxial cable, and results were recorded.

To evaluate antenna performance under realistic conditions, transmission measurements (S_{21}) were conducted with the antennas positioned on opposite sides of the fabricated breast phantom, with and without the inclusion of a tumour. This configuration reflects the practical scenario of a wearable microwave imaging system for non-invasive tumour detection. The VNA was recalibrated for 2-port measurement prior to S_{21} testing. The antennas, labelled ANT 1 and ANT 2, were mounted on a custom holder to maintain stable and consistent alignment during measurements which illustrated in Figure 10. RF cables and SMA connectors also facilitated the connection of antenna to the VNA.

The holder was fabricated using Polylactic Acid (PLA), a material widely cited in microwave literature for its low relative permittivity $\varepsilon_r = 2.7$ and negligible loss tangent (below 0.02), hence it is relatively transparent to the electromagnetic field compared to the high-loss breast phantom. To further minimize potential interference, the holder was designed with a low-profile geometry that secures the antennas solely at the non-radiating ground edges and SMA connectors, ensuring the active aperture and direct signal path remain unobstructed. Besides, the holder serves as a systematic constant across all experimental scenarios. Since the primary objective of this study is to quantify the relative differential in S-parameters between 'tumour-present' and 'tumour-absent' states, any minor static loading introduced by the holder is identical in both configurations settings and effectively cancels out as it remain fixed variables during the comparative analysis, leaving the response variable of the measured contrast attributable solely to the dielectric properties of the tumour.

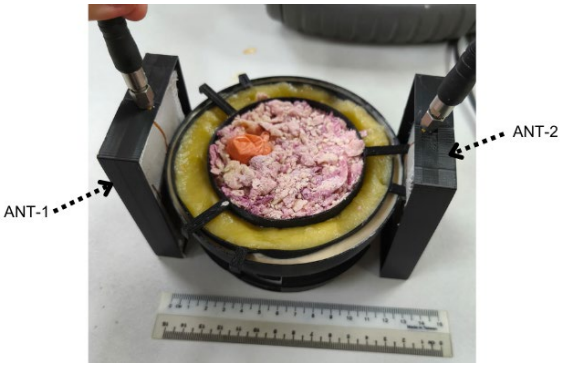

FIGURE 10. S_{21} measurement with both antenna and breast phantom

III. RESULTS AND DISCUSSION

(I). ANTENNA IN FREE SPACE CONDITION (S_{11} ANALYSIS)

A. SIMULATION RESULTS

The proposed design is characterized as a multi-wideband antenna, covering both the lower ISM band and higher frequency microwave bands, as shown in Figure 11. It demonstrates deep resonance minimum of –27.96 dB at 2.4 GHz and –45.28 dB at 5.7 GHz. It achieves a fractional bandwidth of 290 MHz (12%) at the lower band (2.4 GHz), and a significantly broader upper band bandwidth of 6.96 GHz (81.69%) extending from 5.04 GHz. To assess high-frequency viability, the simulation range was extended up to 50 GHz. Results indicate a continuous wideband response of 44.96 GHz (163.37%), covering the entire range from 5.04 to 50 GHz which is shown in Figure 12. This exceptionally wide bandwidth makes the antenna suitable not only for ISM-band tumour detection but also for broader high-frequency applications. However, for the specific purpose of this study which is biomedical sensing, the primary focus remains on the 1 – 9 GHz range, which encompasses the critical tissue penetration capability of the 2.4 GHz band and the high-resolution scattering sensitivity of the 5 – 6 GHz band.

The radiation performance of Ant-4, as depicted in Figure 13, exhibits a strong directional pattern centered at 2.4 GHz. The measurement was taken at 45° intervals. It achieves a peak gain of 5.64 dBi and a suppressed back lobe around –8 dBi, resulting in a front-to-back ratio (FTBR) of 13.64 dB. This hemispherical radiation pattern concentrates energy in the forward half-space, reducing backward exposure and enhancing energy confinement, which is beneficial for microwave imaging applications. The directional characteristics support accurate tumour localization and reduce radiation effect to healthy tissues.

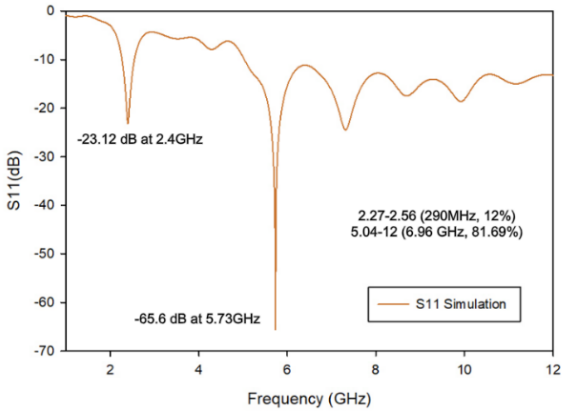

FIGURE 11. S_{11} results of final design

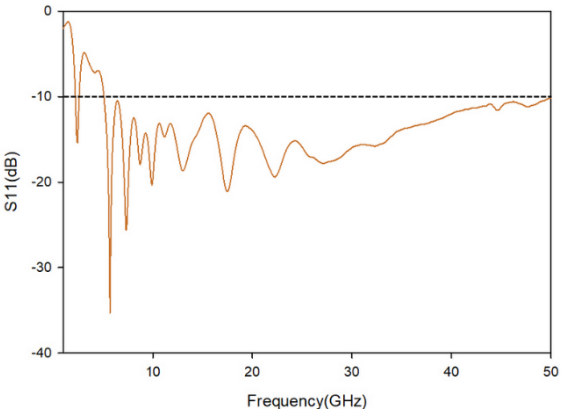

FIGURE 12. S_{11} results (extended to 50 GHz)

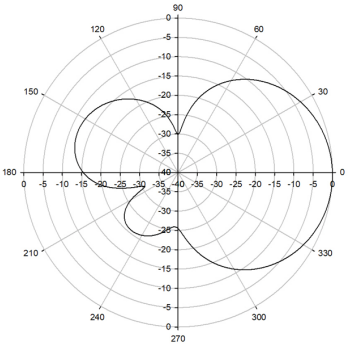

FIGURE 13. Polar plot of the final design

B. PERFORMANCE OF FABRICATED ANTENNA

To validate the performance of the fabricated antenna, reflection coefficient (S_{11}) measurements were carried out in free space using a Vector Network Analyzer (VNA). The results were then compared with the CST simulation results to compare practical implementation and theoretical design. The VNA was operated within a 1 – 9 GHz range, which effectively covered the key frequency bands of interest for this study (ISM and C-band). At 2.4 GHz, the simulated results illustrated in Figure 14 showed a clear resonance below –10 dB, whereas the measured response was shallower. The measured –10 dB bandwidth (4.98–7.4 GHz) was also narrower than the simulated range (5.04–9 GHz), could be attributed to the factor of human handling during the measurement process, such as holding the cables by hand may have introduced variability and affected the consistency of the radiation pattern readings. Crucially, while the measured resonance at 2.4 GHz was less pronounced than the simulation, the antenna maintained excellent performance in the 5 – 6 GHz range. The fabricated prototype showed a prominent resonance near 5.46 GHz (slightly shifted from the simulated 5.7 GHz). This confirms that while the antenna retains functionality at the 2.4 GHz design point, its most robust impedance matching in a practical wearable form factor is achieved in the C-band, supporting a multi-band operational strategy.

As shown in Figure 15, a comparison between the simulated and measured radiation patterns at 2.4 GHz reveals good qualitative agreement in the overall directional behaviour, though notable discrepancies are present. The simulated pattern (dashed blue line) exhibits a clean, symmetrical forward-facing lobe with significantly suppressed side lobes, demonstrating the ability of antenna to focus energy directionally which an essential characteristic for microwave imaging. In contrast, the measured pattern (solid red line) retains a generally forward-directed radiation trend but exhibits noticeable distortion and asymmetry. The main lobe in the measurement is broader and less defined, with several side lobes rising as high as –5 dB compared to –12 dB in the simulated result. This degradation in front-to-back ratio and the presence of higher side lobes are likely attributed to fabrication inaccuracies such as slight crumpling of the copper sheet and limitations in manual cutting precision. In addition, variations in material properties and potential air gaps between layers introduced during manual fabrication may have contributed to the altered current distribution. Despite these deviations, the measured pattern still confirms the antenna directional radiation capability under practical wearable conditions. These differences emphasize the importance of considering mechanical and fabrication tolerances in flexible antenna design, while also validating the robustness and functional performance of antenna in real-world environments.

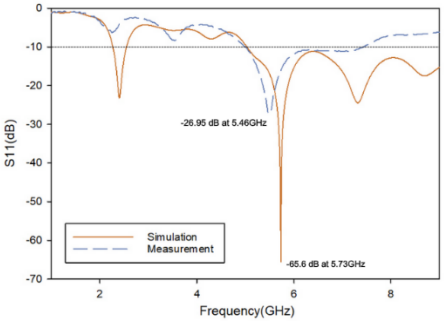

FIGURE 14. S_{11} simulation vs measurement results

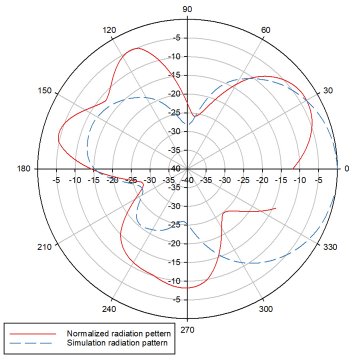

FIGURE 15. Radiation pattern (simulation vs measurement)

(II). ANTENNA WITH BREAST PHANTOM (S_{21} ANALYSIS)

A. SIMULATION RESULTS

To evaluate the detection capabilities of the proposed antenna in a realistic biomedical environment, several simulations was performed using a multilayer breast phantom model. The simulations focused on analysing the variation in the transmission coefficient (S_{21}) under different conditions: (i) free space (absence of phantom or tumour), (ii) phantom without tumour, (iii) phantom with tumour, (iv) various tumour sizes and locations and (v) different air gap configurations between the antenna and the phantom. Figure 16 illustrates the simulation setup, where a dual-pair antenna is placed around the breast phantom with an embedded tumour to replicate the tumour detection scenario. Figure 17 demonstrates the flexibility of antenna, showing how it conforms to the curvature of the breast phantom, which is essential for ensuring effective coupling and stable measurements in wearable biomedical applications.

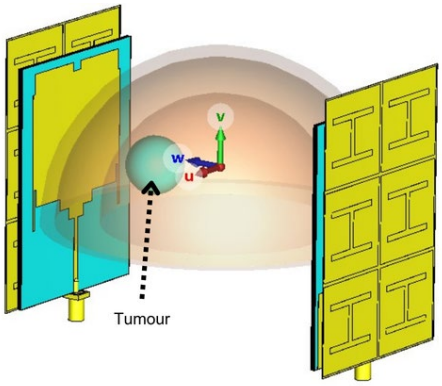

FIGURE 16. Simulation setup of dual pair antenna with breast phantom

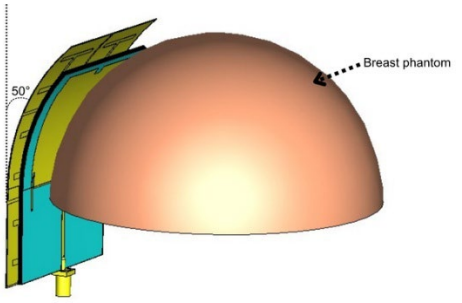

FIGURE 17. Bending antenna follows the shape of breast phantom

Subsequently, the antenna was simulated in proximity to a 120 mm diameter breast phantom to evaluate transmission performance under wearable conditions. Two air gap configurations were analysed: 0 mm (direct contact) (Figure 18) and 1.5 mm (representing realistic separation due to clothing or imperfect attachment) (Figure 19). The results illustrated in Figure 20 and Figure 21 demonstrated that the 0 mm air gap condition yielded a significantly deeper S_{21} resonance dip of –85.7 dB at 3.53 GHz, compared to –51.2 dB at 3.74 GHz in the tumour-absent scenario, there is a clear indication of strong electromagnetic interaction with the lossy tissue. In contrast, the 1.5 mm air gap condition exhibited less pronounced variation between tumour and non-tumour cases, with a minimum S_{21} of –52.39 dB, indicating reduced coupling and lower sensitivity to dielectric contrast.

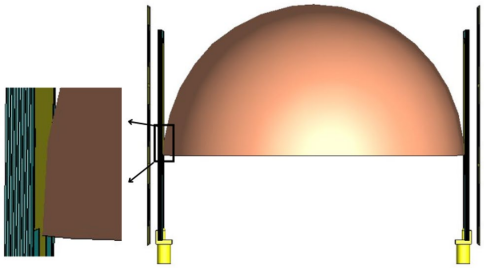

FIGURE 18. Direct contact configuration

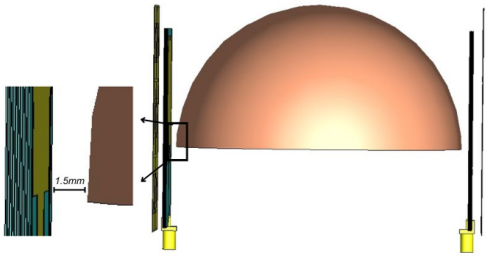

FIGURE 19. 1.5mm air gap configuration

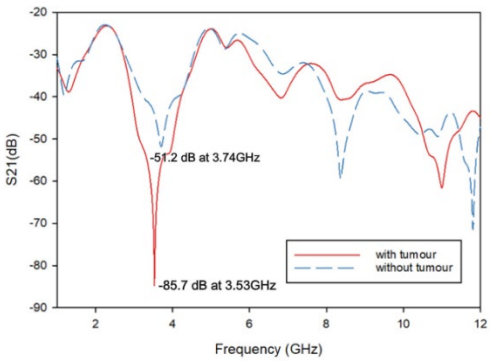

FIGURE 20. S_{21} result with antenna in direct contact with breast phantom (with and without tumour)

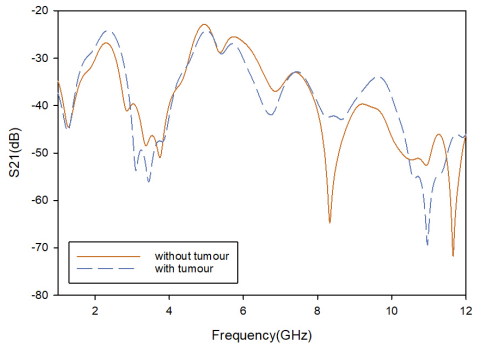

FIGURE 21. S_{21} result with a 1.5 mm air gap between antenna and breast phantom (with and without tumour)

These results confirm that direct contact enhances signal transmission loss and tumour detectability, as the antennas near field can more effectively interact with internal tissue structures. The air gap, acting as a low-permittivity spacer, reduces near-field penetration, which weakens the antenna ability to sense internal dielectric variations. Therefore, the 0 mm air gap configuration was selected for subsequent simulations as it represents an idealized but achievable reference scenario for tightly worn or adhesive-mounted devices. Although perfect contact may not always be attainable in practice, this setup provides a consistent benchmark to evaluate maximum detection sensitivity.

A parametric sweep was conducted to investigate the effect of tumour size, ranging from 2 mm to 10 mm in radius, with the results presented in Figure 22. The simulation showed that as the tumour radius increased, the S_{21} resonance became progressively deeper, indicating stronger electromagnetic interaction with the larger dielectric volume. Specifically, the minimum S_{21} value shifted from –69.41 dB for a 2 mm tumour to –84.6 dB for a 10 mm tumour. This trend confirms that larger tumours introduce greater perturbations in the signal path, thereby enhancing detectability.

Additionally, the effect of tumour location with different distance was analysed, with tumour of radius 2 mm as shown in Figure 23. The results revealed that S_{21} variations were more significant when the tumour was positioned closer to the antenna, due to stronger coupling with the near-field region. This confirms that the antenna is highly sensitive to localized dielectric changes in the immediate vicinity, which is a desirable characteristic for early-stage tumour detection in wearable microwave imaging systems.

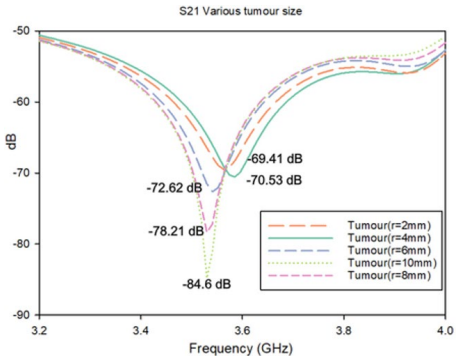

FIGURE 22. S_{21} results for parametric sweep of tumour size from 2 mm to 10 mm positioned near to the antenna

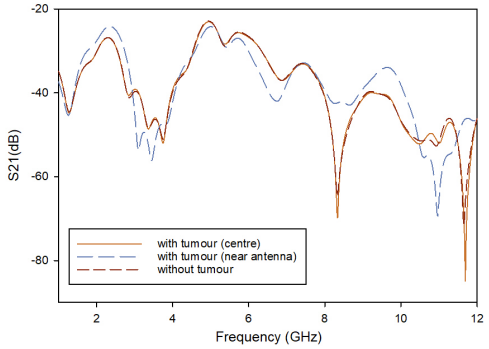

FIGURE 23. S_{21} results for different tumour locations (centre and near the antenna)

B. PERFORMANCE OF FABRICATED ANTENNA

The S_{11} and S_{21} measurement results illustrated in Figure 24 provide complementary insights into the performance of antenna, particularly its capability for breast tumour detection using microwave signals. In this study, the antenna was initially designed with a focus on 2.4 GHz, a common ISM band known for its tissue penetration and safety. While this frequency was the starting point for development, the experimental data identifies several high-sensitivity regions (highlighted in orange in Figure 24) where the antenna strongest performance emerged at higher frequencies, particularly in the 5.67 – 6.2 GHz range, demonstrate that the optimal diagnostic strategy utilizes a multi-band approach. These regions designate specific spectral intervals where the antenna system exhibits maximized sensitivity to dielectric perturbations, effectively representing the highest Signal-to-Clutter Ratio (SCR). In this context, the "signal" constitutes the scattering caused by the tumor, while the "clutter" represents the background reflections from the healthy breast tissue and phantom interfaces.

This shift in focus from a single-band 2.4 GHz operation to a multi-band detection scheme is supported by the physics of microwave imaging. Lower frequencies (2.4 GHz) generally offer better penetration but lower resolution, while higher frequencies (5 – 6 GHz) provide the shorter wavelengths necessary to resolve small dielectric anomalies (tumours).

Consequently, the primary region of interest occurs between 5.67 and 6.2 GHz. Within this band, the S_{11} response shows excellent impedance matching (well below –10 dB), creating a condition of impedance loading. In this region, the S_{11} resonance aligns with the S_{21} peak, indicating that the antenna is efficiently coupled to the phantom. The orange box highlights where the tumour presence induces a measurable shift in magnitude, proving that the antenna near-field is effectively interacting with the inclusion.

This strong contrast validates the antenna highly sensitive to dielectric changes caused by tumour presence, confirming its effectiveness as a diagnostic tool. Notably, this frequency range also aligns with enhanced field interaction and deeper signal penetration within the breast phantom.

Additionally, the orange markers at 2.82–3.41 GHz and 8.41–9.00 GHz in the Figure 24 highlight secondary bands of sensitivity driven by broadband scattering. Despite less significance resonance notches in these regions, the S_{21} responses still exhibit a distinct delta between the different phantom conditions. These observations suggest that the antenna benefits from multi-band performance, where even in regions with less prominent S_{11} notches, internal reflections and scattering contribute to tumour detectability.

Although the antenna performance at 2.4 GHz can be further optimized in future iterations, it is encouraging that the tumour-present case still shows a slightly lower S_{21} magnitude, indicating the antenna ability to interact with tissue variations even at the initial target frequency. Importantly, these results confirm that the antenna is not only limited to a single band but provides reliable tumour sensitivity across a broad frequency range.

In summary, the study validates a multi-wideband detection methodology. While 2.4 GHz guided the initial design, the measurement outcomes at 5.67–6.2 GHz and other secondary bands reveal that the antenna achieves strong practical performance, with broad tissue sensitivity and clear tumour discrimination, paving the way for further enhancements and robust diagnostic potential.

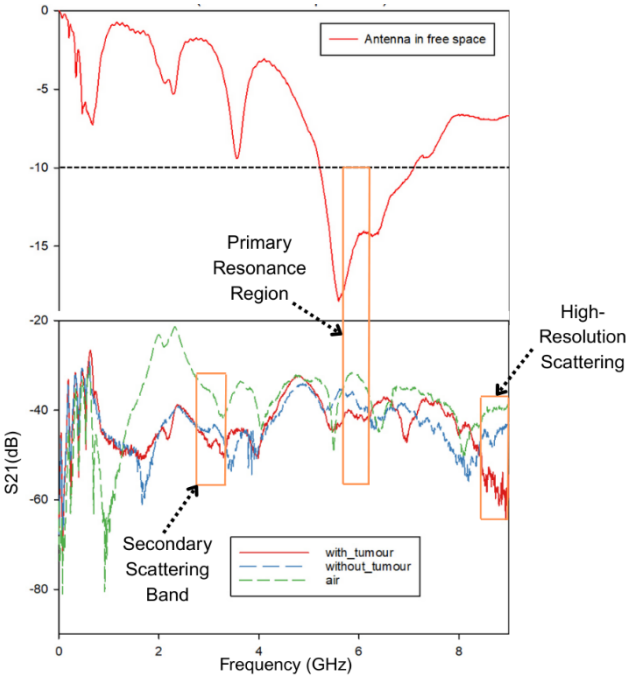

FIGURE 24. S_{11} and S_{21} measurement results among 3 scenarios (air, with tumour at tumour size of 5mm radius and without tumour)

(III). SAR ANALYSIS (WITH BREAST PHANTOM)

To ensure compliance with electromagnetic exposure limits and assess safety for wearable use, Specific Absorption Rate (SAR) analysis was conducted at 2.4 GHz using CST Studio Suite licensed version. The anatomically realistic "Donna" model was used and a breast section including skin, fat, glandular tissue was extracted for focused simulation.

The final antenna design was evaluated in direct contact with the breast phantom. The simulation employed the actual system input power of 0.04 W (40 mW). Under these conditions, the maximum localised SAR averaged over 10 g of tissue was 0.23 W kg^{-1}, which is an order of magnitude below the ICNIRP general-public limit of 2 W kg^{-1}. The SAR distribution (See Figure 25) shows that absorption is confined to a small region beneath the radiating edge, while the surrounding tissue remains below 0.05 W kg^{-1}. The low SAR value observed is consistent with the shielding properties of metamaterials. As noted in literature reviews of AMC applications, the inclusion of an AMC ground plane in Medical Body Area Networks (MBAN) can significantly reduce SAR by isolating the human body from electromagnetic radiation. In this design, the AMC array effectively blocks backward radiation toward the breast tissue, ensuring the system remains well within the ICNIRP safety limits [21]. Although only simulation data are presented, the use of a detailed, multilayer anatomical model and the application of the actual transmit power provide strong evidence that the antenna is inherently safe for continuous real-time wearable diagnostics without exceeding regulatory exposure limits.

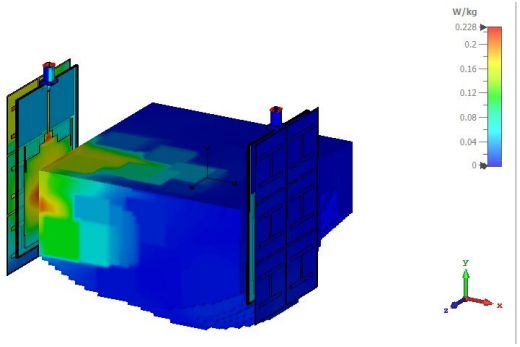

FIGURE 25. SAR simulation when breast tumour is inserted

(IV). BENDING ANALYSIS (WITH BREAST PHANTOM)

Given the flexible nature of the cotton-based substrate, bending performance was evaluated to assess the impact of mechanical deformation on reflection coefficient (S_{11}). Simulations were conducted in CST Microwave Studio with the antenna wrapped around curved surfaces representing the breast contour at bending angles of 50° and 60°, in comparison to the 0º condition which depicted in Figure 26.

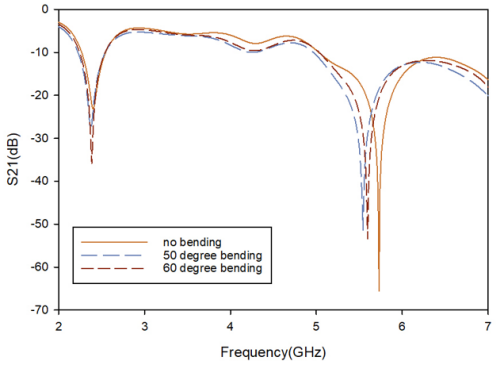

FIGURE 26. The comparison of 0°, 50° and 60° antenna bending condition

In the flat condition (0°), the antenna exhibited a strong resonance at 5.71 GHz with an S_{11} value of –44.89 dB, indicating excellent impedance matching. When bent to 50°, the main resonance shifted slightly leftward to 5.54 GHz, accompanied by a deeper return loss of –50.76 dB. Further bending to 60° produced a minimal shift to 5.60 GHz, with an even lower S_{11} of –53.01 dB. Despite these shifts, reflection coefficient remained well below –10 dB across the entire wideband range, confirming that impedance bandwidth was unaffected. As illustrated in Figure 26, both 50° and 60° bends caused minor frequency shifts, including around 2.4 GHz, with slightly deeper resonances. Interestingly, the 50° bend exhibited a more noticeable shift than the 60°, likely due to non-uniform strain distribution affecting the effective electrical length of the antenna. These results clearly demonstrate the insensitivity of antenna to bending and deformation, a critical feature for wearable biomedical applications, where antennas must tolerate continuous bending, compression and repositioning due to body movement. The ability to maintain stable performance under such dynamic conditions ensures consistent signal acquisition and measurement reliability, making the antenna highly suitable for real-time, on-body microwave imaging and diagnostics.

IV. COMPARISON OF PROPOSED MULTI-WIDEBAND ANTENNA WITH EXISTING ANTENNAS

The comparative analysis of the proposed multi-wideband antenna with existing antennas from previous research is summarized in Table IV. The comparison focuses on key performance parameters including frequency range, bandwidth, radiation pattern at 2.4 GHz, tumour detection capability, number of antennas used, specific absorption rate (SAR) and bending effect. Although the initial design target of this study was 2.4 GHz, most existing works operating at this frequency reported omnidirectional radiation patterns. In contrast, the proposed antenna demonstrates a directional pattern at 2.4 GHz, allowing more focused energy delivery into breast tissue and reduced backward radiation. While the measured S_{11} at 2.4 GHz did not fall below the –10 dB threshold, the antenna still exhibited tumour sensitivity through observable S_{21} variations, indicating functional interaction with dielectric contrast at low frequencies.

More notably, measurements confirmed that the antenna performs optimally in the 5.67–6.2 GHz band which has a clearer distinction in S_{21} between tumour-present and tumour-absent scenarios. For instance, Mahfuz *et al.* [19] reported a significant –19.128 dB S_{11} for a healthy phantom at 5.77 GHz, reflecting strong impedance matching. A UWB textile monopole sensor in another study [20] able to detect tumour at 4.7 and 6.2 GHz, supporting the diagnostic value of the higher-frequency region even for single-element antennas. Additionally, Abouelnaga *et al.* [9] implemented a four-element circular MIMO antenna that accurately localized tumours at multiple resonances, including 5.83 GHz.

These comparisons highlight that the proposed design not only complements the capabilities of existing antennas but also exceeds them in key aspects. Its dual-band coverage (2.27–2.56 GHz and 5.04–50 GHz) allows both low-frequency and high-resolution operation. Safety-wise, it demonstrates excellent SAR compliance with a low value of 0.23 W/kg averaged over 10 g, which is well below the 2 W/kg ICNIRP safety limit, making it highly suitable for continuous wearable use. Structurally, the antenna maintains consistent electric performance under up to 60° of bending, outperforming many prior designs that experienced signal degradation at lower bending angles. Functionally, it effectively detects tumours ranging from 2 mm to 10 mm in radius using S_{21} transmission responses, whereas several previous studies relied solely on S_{11} −based detection with narrower tumour size ranges. Overall, the comparison validates the proposed antenna practical relevance, robustness, and diagnostic reliability which particularly in the 5–6 GHz band where its measured performance is most prominent.

TABLE IV. Comparison between Previous Studies and Proposed Antenna

Ref.	Frequency (GHz)	BW (GHz)	Radiation Pattern (2.4 GHz)	Tumour Detection capability	No. of antennas used	SAR value (W/kg) (10 g)	Bending effect to S_{11}
[9]	2.4-10.6	8.2	Directional (2.4 & 5.8 GHz)	Yes (10mm radii)	4	1.75	S_{11} above -10 dB at certain frequency
[8]	3.1-10.6	7.5	Omnidirectional	Yes (2mm radii via S_{11} only)	1	-	10° angle has lesser impedance bandwidth
[7]	1-12	11	Omnidirectional	Yes (5 - 35mm radii)	2	0.2	Insensitive up to 45°
[17]	2.26 - 13.71	11.45	Omnidirectional	Yes (4,5 mm radii via S_{11} only)	1	0.93 (1g)	Insensitive up to Rx = 25 mm
[19]	5.74 - 5.87	0.13	Directional (5.8 GHz)	Yes (10-30mm radii via S_{11} only)	1	0.419	Insensitive up to r = 50mm
[20]	1.8-10	8.2	-	Yes (5-20mm radii)	2	0.58	-
Proposed	2.27 - 2.56, 5.04 -50	0.29, 44.96	Directional	Yes (2 – 10 mm radii)	2	0.23	Insensitive up to 60°

V. CONCLUSION

In conclusion, a flexible multi-wideband wearable antenna for breast tumour detection using microwave imaging was successfully designed, simulated, fabricated, and evaluated. The antenna was developed to achieve a directional radiation pattern at 2.4 GHz while maintaining low profile and consistent performance under bending and proximity to human tissue. It demonstrated good return loss ($S_{11} < -10$ dB) across the UWB range, and with the integration of an Artificial Magnetic Conductor (AMC), achieved higher gain, supporting multi-wideband operation that encompasses a 290 MHz bandwidth at the 2.4 GHz ISM band and a continuous upper band extending up to 44.96 GHz. Measurements using a realistic breast phantom confirmed its directional radiation capability and the SAR value remained low at 0.23 W/kg (10 g), well within the ICNIRP safety limit. The antenna also successfully detected breast tumours of various sizes (2-10 mm radius) with measurable variations in transmission coefficient (S_{21}), indicating its potential to identify not only the presence but also the size of tumours. Lastly, it maintained stable performance under bending angles of 0°, 50° and 60°, demonstrating its insensitivity to deformation, validating its suitability for real-time wearable diagnostics. Future work will focus on extending the bandwidth below 5 GHz and miniaturising the structure for enhanced early-stage diagnosis.

ADKNOWLEDGEMENT

The authors would like to thank the Ministry of Higher Education (MOHE), School of Postgraduate Studies (SPS), Research Management Centre, Advanced RF and Microwave research group, IJN-UTM Cardiovascular Engineering Centre and Universiti Teknologi Malaysia (UTM) Johor Bahru for the support of the research under Fundamental Research Grant Scheme FRGS/1/2023/TK07/UTM/02/23, and UTM Fundamental Research Grant Q.J130000.3823.24H07. We sincerely thank the Radar Laboratory, Advanced Microwave and Antenna Laboratory (AMAL), and Basic Microwave Laboratory for providing the facilities and equipment for our antenna prototype through S-parameter and radiation pattern measurements. Special thanks to Mrs. Mustiah binti Tuiman and Mr. Mohd Fikri bin Ismail for their valuable assistance during the measurement process.

REFERENCES

[1] F. A. ali abdulla and A. Demirkol, "A novel textile-based UWB patch antenna for breast cancer imaging," Phys Eng Sci Med, Sep. 2024, doi: 10.1007/s13246-024-01409-w.W.-K. Chen, *Linear Networks and Systems*. Belmont, CA, USA: Wadsworth, 1993, pp. 123–135.

[2] D. N. Elsheakh, R. A. Mohamed, O. M. Fahmy, K. Ezzat, and A. R. Eldamak, "Complete Breast Cancer Detection and Monitoring System by Using Microwave Textile Based Antenna Sensors," *Biosensors (Basel)*, vol. 13, no. 1, Jan. 2023, doi: 10.3390/bios13010087.

[3] Y. Rahayu, Rosdiansyah, M. F. Hilmi, and T. Odih, "Wearable Antenna for Time-Domain Breast Tumor Detection," *International Journal of Technology*, vol. 12, no. 6, pp. 1101–1111, 2021, doi: 10.14716/IJTECH.V12I6.5187.

[4] M. A. Shahira Banu, S. Vanaja, and S. Poonguzhali, "UWB microwave detection of breast cancer using SAR," in *2013 International Conference on Energy Efficient Technologies for Sustainability, ICEETS 2013*, 2013, pp. 113–118. doi: 10.1109/ICEETS.2013.6533366.

[5] F. E. Zerrad *et al.*, "Microwave Imaging Approach for Breast Cancer Detection Using a Tapered Slot Antenna Loaded with Parasitic Components," *Materials*, vol. 16, no. 4, Feb. 2023, doi: 10.3390/ma16041496.

[6] V. L. N. P. Ponnapalli, S. Karthikeyan, and J. L. Narayana, "A Circular Slotted Shaped UWB Monopole Antenna for Breast Cancer Detection," 2022.

[7] Ç. Kurnaz, F. Alsharif, and A. A. Cheema, "Determination of the breast cancer tumor diameter using a UWB microwave antenna system," *Sigma Journal of Engineering and Natural Sciences*, vol. 41, no. 5, pp. 999–1012, Oct. 2023, doi: 10.14744/sigma.2023.00047.

[8] A. H. Rambe, M. Jusoh, S. S. Al-Bawri, and M. A. Abdelghany, "Wearable UWB Antenna-Based Bending

and Wet Performances for Breast Cancer Detection," *Computers, Materials and Continua*, vol. 73, no. 3, pp. 5575–5587, 2022, doi: 10.32604/cmc.2022.030902.

[9] T. G. Abouelnaga, E. K. I. Hamad, S. A. Khaleel, and B. Beiranvand, "Defining Breast Tumor Location Using a Four-Element Wearable Circular UWB MIMO Antenna Array," *Applied Sciences (Switzerland)*, vol. 13, no. 14, Jul. 2023, doi: 10.3390/app13148067.

[10] U. Ali, S. Ullah, B. Kamal, L. Matekovits, and A. Altaf, "Design, Analysis and Applications of Wearable Antennas: A Review," 2023, *Institute of Electrical and Electronics Engineers Inc.* doi: 10.1109/ACCESS.2023.3243292.

[11] N. M. Zain, M. A. Aris, and H. Ja'afar, "Effect of Conductive Materials and Substrates for Flexible Patch Antennas: A Comprehensive Review," in *2021 IEEE Asia-Pacific Conference on Applied Electromagnetics, APACE 2021*, Institute of Electrical and Electronics Engineers Inc., 2021. doi: 10.1109/APACE53143.2021.9760568.

[12] B. Almohammed, A. Ismail, and A. Sali, "Electro-textile wearable antennas in wireless body area networks: materials, antenna design, manufacturing techniques, and human body consideration—a review," Mar. 01, 2021, *SAGE Publications Ltd*. doi: 10.1177/0040517520932230.

[13] D.Xu, Z.Wang, Y.Wang, and J.Wu, "A high performance ultra-wideband low cost SMA-to-GCPW transition," *IEEE Trans Microw Theory Tech*, vol. 24, no. 1, pp. 47–48, 2016, doi: 10.1109/TMTT.1976.1128765.

[14] Garg, R. (2001). Microstrip antenna design handbook. Artech house.

[15] Mersani, A., Lotfi, O., & Ribero, J. M. (2018). Design of a textile antenna with artificial magnetic conductor for wearable applications. Microwave and Optical Technology Letters, 60(6), 1343-1349.

[16] A. H. Rambe, M. Jusoh, S. S. Al-Bawri, and M. A. Abdelghany, "Wearable UWB Antenna-Based Bending and Wet Performances for Breast Cancer Detection," *Computers, Materials and Continua*, vol. 73, no. 3, pp. 5575–5587, 2022, doi: 10.32604/cmc.2022.030902.

[17] A. B. Dey and W. Arif, "Design and analysis of a CPW-fed flexible ultrawideband antenna for microwave imaging of breast cancer," *International Journal of RF and Microwave Computer-Aided Engineering*, vol. 32, no. 9, Sep. 2022, doi: 10.1002/mmce.23262.

[18] F. E. Zerrad et al., "Symmetrical and Asymmetrical Breast Phantoms With 3D-Printed Anatomical Structure for Microwave Imaging of Breast Cancer," IEEE Access, vol. 10, pp. 96896–96908, 2022, doi: 10.1109/ACCESS.2022.3205004.

[19] Mahfuz, M. H., Islam, M. R., Malek, N. F. A., Habaebi, M. H., Sakib, N., & Baladi, E. (2025). Wearable Textile Patch DSSRS Antenna for Body Tumors Detection with Reduced SAR. IIUM Engineering Journal, 26(1), 148-168.

[20] Elsheakh, D. N., Mohamed, R. A., Fahmy, O. M., Ezzat, K., & Eldamak, A. R. (2023). Complete breast cancer detection and monitoring system by using microwave textile based antenna sensors. Biosensors, 13(1), 87.

[21] Dewan, R., Rahim, M. K. A., Hamid, M. R., Yusoff, M. F. M., Samsuri, N. A., Murad, N. A., & Kamardin, K. (2017). Artificial magnetic conductor for various antenna applications: An overview. *International Journal of RF and Microwave Computer-Aided Engineering*, *27*(6), e21105.

[22] Jalil, M. E., Rahim, M. K. A., Samsuri, N. A., Dewan, R., & Kamardin, K. (2017). Flexible ultra-wideband antenna incorporated with metamaterial structures: multiple notches for chipless RFID application. *Applied Physics A*, *123*(1), 48.